ORIGINAL PAPER

Nonlinear modeling of combined galloping and vortex-induced vibration of square sections under flow

Peng Han · Pascal Hémon · **Guang Pan** ·
Emmanuel de Langre

Abstract In this paper, we propose a model for the transverse oscillation of a square-section cylinder under flow. The fluctuating transverse force due to vortex shedding is represented using a coupled nonlinear wake oscillator, while the unsteady force for galloping caused by the varying incidence angle effects is modelled using the quasi-steady approach. First, we analytically investigate the lift behavior and phase angle variation of the square cylinder under forced vibrations. Comparison with experimental data is used to determine the form of the coupling terms and its values. The present model shows advantages in predicting the phase angle, and it successfully captures the change in sign of the phase. Second, the proposed model is directly applied in predicting free oscillation cases without any tuning. The dynamical behaviors predicted by this model are compared with published experiments under different Scruton numbers, and reasonable agreement can be found. The results indicate that the model can not only be applied in simulating the "pure galloping" and "pure VIV," but also is able to capture the interactions of VIV and galloping, including combined and separate VIV-galloping motions.

P. Han · G. Pan
School of Marine Science and Technology, Northwestern
Polytechnical University, Xi'an 710072, China

P. Han · P. Hémon · E. de Langre (✉)
LadHyX, Ecole polytechnique, CNRS, Institut
Polytechnique de Paris, 91128 Palaiseau, France
e-mail: delangre@ladhyx.polytechnique.fr

1 Introduction

When a deformable body is submitted to flow, it will vibrate and in turn affect the fluid flow. This well-known phenomenon is called flow-induced vibration (FIV) and may occur in many fields of engineering, such as civil engineering (chimneys and bridges), off-shore engineering (risers and pipes), and energy engineering (electrical cables and power lines); it is therefore of practical interest [1]. There are many forms of FIV, but in this paper, we focus on vortex-induced vibration (VIV) and galloping [2].

VIV is a self-limited motion induced by vortex shedding from a bluff body. The most important feature of VIV is "lock-in," during which both the vortex shedding frequency and the oscillation frequency are locked [3]. For flow velocities outside the lock-in range, the amplitude of motion is small. Studies on VIV are mainly for a circular-shape cylinder, because it could vibrate in pure VIV, away from the influence of other vibrations, such as galloping [1]. In past decades, a large body of experimental studies have been carried out on VIV of a circular cylinder, see reviews by Bearman [3], Williamson and Govardhan [4], and Sarpakaya [5]. Computing VIV has been considered as a challenging problem due to the complex nonlinear interactions between the fluid and solid dynamics. Simulations,

such as with the DNS method, has been employed to predict VIV [6]. Although DNS allows to obtain details on the fluid flow, it is difficult to apply in complicated flow conditions and in three-dimensional cases. Consequently, reduced order models based on the simple idea of a wake oscillator can be useful and efficient tools to describe such vibrations. In those reduced order models, the lift acting on a circular cylinder caused by vortex shedding is simulated by a self-excited oscillator, which satisfies the Rayleigh or van der Pol equation, or some modified forms of them [7–9]. Facchinetti et al. [10] proposed a wake oscillator model using a single flow variable coupled to the structural oscillator by acceleration, to describe the fluctuating nature of the vortex shedding. This model is simple to use and has been shown to simulate VIV both quantitatively and qualitatively for elastically supported rigid cylinders. This approach was then extended to its 3D version and has been applied with success in analyzing the vibration behaviors of flexible and slender cylinders under uniform and shear flow [11–14]. It should be noted here that wake oscillators, which were originally introduced as purely phenomenological (see the review in [15]) have later been related to the unsteady fluid dynamics downstream of the bluff body by several approaches. See for instance in [16] the relation to the dynamics of the dead fluid region, in [17] the relation to Navier-Stokes equations and in [18] the relation to the linear stability of the coupled wake/solid system. We use here the van der Pol wake oscillator, one of the simplest and most used form.

Galloping is also a self-limited vibration but the amplitude of the limit cycle always increases with the flow velocity, contrary to VIV. The galloping instability can be understood by considering the variations of the instantaneous incidence angle [2]. Thus, cylinders with circular cross section, are not subject to galloping. Square section is the ideal shape, not only because of its known galloping instability, but also because it is one of the most common geometries in engineering. By using the quasi-steady theory (QST), Parkinson and Smith [19] predicted transverse galloping for a square cylinder, and particularly the critical velocity, U_g, above which galloping occurs. Their results showed good agreement with experimental data. Later, this model has been widely used to predict the galloping motion at a high reduced velocity, in different ranges of physical parameters (for instance, in the low Reynolds number (Re) range [20], in the high Re range [21,22],

with different turbulence intensity in these same references). Also, this model has been used in modeling piezoelectric energy harvesting from oscillating cylinders with square shapes [23,24].

VIV and galloping are therefore two distinct mechanisms that cause motions of elastically supported square cylinder. Depending on the parameters of the flow and of the solid, the effects of VIV and galloping may overlap or not. We need a simple and efficient mathematical model to predict combined VIV and galloping in the most general cases. The approaches cited above with a wake oscillator for VIV and a QST model for galloping are good candidates to build such a combined model. Some attempts have been made in this direction. Bouclin [25] combined two force terms related to VIV (developed by [7]) as well as galloping (developed by [19]) and applied the model to the case of a square cylinder. Corless and Parkinson [26] slightly modified Bouclin model and employed multiple scales method to solve the equations. Tamura and Shimada [27] proposed a model for the square cylinder by adding quasi-steady force term in the previous model developed by Tamura and Matsui [16] for a circular cylinder. They used a time-dependent variable, based on Birkhoff's oscillator model for the dead air region behind a cylinder, to describe the transverse force caused by vortex shedding. This model was applied in simulating energy harvesting of a square cylinder by Andrianne et al. [24]. Both Corless and Parkinson's model as well as Tamura and Shimada's model has been extended to be applied in predicting VIV and galloping of rectangular cylinders by Mannini et al. [28]. Recently, Liu et al. [29] developed two new approaches by modifying Corless and Parkinson's model and adding the fluid inertia effect.

Considering that the wake oscillator approach by Facchinetti et al. [10] is simple and efficient, we propose, following the same idea as the work above, to extend Facchinetti et al.'s model for a square cylinder and then combine it with a QST model of galloping. In this paper, the dynamic equations based on Facchinetti et al's model for transverse vibration of a square cylinder are developed in Sect. 2. In Sect. 3, the model is investigated analytically with different coupling terms and then applied in simulating lift characteristics and phase angle variations of a forced vibration case. Furthermore, coupling parameters are estimated from experimental data considering forced vibrations. In Sect. 4, the model is employed to cap-

ture free vibration responses of a square cylinder under different Scruton numbers (S_c), corresponding to overlap or not between VIV and galloping. A comparison between the numerical and experimental results is also presented in this section. Finally, discussion and conclusions are made in Sects. 5 and 6, respectively

2 Mathematical model

First, the main features of the model proposed by Facchinetti et al. [10] are recalled here. Considering an elastically supported rigid circular cylinder under flow, its dynamical responses can be modelled by a typical M-C-K equation, which reads

$$m\ddot{Y} + c\dot{Y} + kY = F_v, \tag{1}$$

where m represents the mass, including both the structural mass, m_s, and the added mass, m_a. Also, c is composed of the viscous dissipations of the system c_s, and the fluid-added damping, $c_f = \gamma \omega_f \rho D^2$. The () stands for time derivation. Here, γ is the stall parameter, which is related to the drag coefficient, C_d, and is assumed constant for simplicity (see [1,8,10]). We introduce ρ, D, k, U, St and ω_f as fluid density, diameter of the cylinder, stiffness, flow velocity, Strouhal number and the vortex shedding frequency expressed as $\omega_f = 2\pi St U/D$, respectively. Note that the parameters m, c, and k are defined per unit length.

The right-hand side force term in Eq. (1) represents the lift caused by vortices. It can be expressed as $F_v = \rho U^2 D C_L^v/2$, where C_L^v is the vortex-induced lift coefficient of an oscillating cylinder. Now, we introduce a variable $q = 2C_L^v/C_{L0}$ as the ratio between the lift coefficient of an oscillating cylinder (C_L^v) and a fixed one (C_{L0}). Here, C_{L0} is obtained by lift measurement from flow over a stationary cylinder. The dimensionless wake variable q can be interpreted as a reduced vortex (or "fluctuating") lift coefficient that satisfies the van der Pol equation [10]. This is common, with some variations, to most of the wake-oscillator models in the literature since the pioneering work of Hartlen and Currie [7]. The equation for the wake oscillator involving variable q can be written as

$$\ddot{q} + \varepsilon \omega_f \left(q^2 - 1\right)\dot{q} + \omega_f^2 q = (A/D)\ddot{Y}, \tag{2}$$
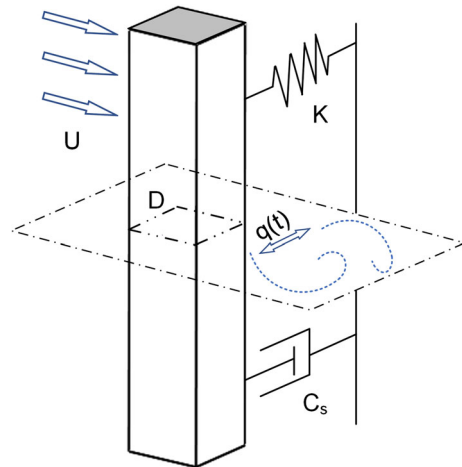

Fig. 1 Elastically supported square cylinder and wake oscillator

where ε and A are two constant parameters, and for more details see [10]. The van der Pol equation or its modified form is commonly used to represent the fluctuating nature of the vortex street [7,10,14,30]. This is because the vortex-shedding process is the result of a hydrodynamic instability and as such can be seen as self-exited and self-limited. The van der Pol equation is the simplest dynamic equation that contains these two important features. In fact, any nonlinear oscillator that generates a limit cycle can potentially be used (and has been used) to represent the vortex-shedding process. The van der Pol equation can represent the most important characteristics of the vortex shedding process, which is considered only through the single variable q, a measure of the effect of the vortex shedding on the lift coefficient.

Now let us turn to the case of a square cylinder, as shown in Fig. 1. Facchinetti et al's model does not include the physics of galloping, but only of VIV. As a result, the lift force related to galloping, F_g, needs to be added in the right side of Eq. (1). Parkinson and Smith [19] demonstrated that the force (F_g) acting on a square cylinder causing galloping can be described by approximating the relation between the lift coefficient (taken from flow over a fixed cylinder) and the incidence angle α. Assuming the velocity for the structural motion $\dot{Y}$ is quite smaller when compared with the incoming flow velocity U, we can therefore use $\dot{Y}/U$ to approximately model the incidence angle ($\dot{Y}/U \approx \alpha$) and further to describe its instantaneous effects. As in Parkinson and Smith [19], a seventh-order polynomial

based on the above assumption is employed here to model the galloping force, which reads

$$F_g = \frac{1}{2}\rho U^2 D C_L^g = \frac{1}{2}\rho U^2 D \cdot [A_1(\dot{Y}/U) - A_2(\dot{Y}/U)^3 + A_3(\dot{Y}/U)^5 - A_4(\dot{Y}/U)^7], \quad (3)$$

where A_i are constants depending on characteristics of the incoming flow (Reynolds number,...), and C_L^g represents the lift coefficient related to galloping. In a given range of flow parameters, the coefficients A_i have been obtained by considering the variation of the lift coefficient on a fixed body with the angle of attack of the incoming flow α, and approximating this variation by polynomials. This lift coefficient can be obtained by experiments or numerical simulations, as was done in [19,20]. In the present paper, for all the subsequent tests, we use values previously given in published studies. For a different range of flow parameters, or different section, it would be necessary to obtain these coefficients A_i from other data on lift coefficients. Finally, the dynamic equations for VIV and galloping of a square cylinder are therefore modelled as

$$m\ddot{Y} + c_s \dot{Y} + kY = F_v + F_g$$
$$\ddot{q} + \varepsilon\omega_f \left(q^2 - 1\right)\dot{q} + \omega_f^2 q = f(Y)/D. \quad (4)$$

Besides the new force term in M-C-K equation in Eq. (4), note that there are also other differences between the model for a square cylinder, Eq. (4), and for a circular one, Eqs. (1) and (2). First, the stall parameter, γ, is deleted in the present model. This is because its effects has already been considered in the first coefficient (A_1) of the expression of C_L^g. Second, the right-hand term in the van der Pol equation is written as a more general function of Y; see later.

We now introduce dimensionless terms, including mass ratio μ, damping ratio ξ, reduced velocity U_r, structural angular frequency ω_s, dimensionless time t, reduced angular frequency δ and dimensionless displacement y, defined as

$$\mu = (m_s + m_a)/\rho D^2, \zeta = r_s/(2m\omega_s)$$
$$U_r = 2\pi U/(\omega_s D), \omega_s = \sqrt{k/m}$$
$$t = T\omega_f, y = Y/D, \delta = \omega_s/\omega_f. \quad (5)$$

Substituting Eq. (5) into Eq. (4) gives

$$\ddot{y} + (2\zeta\delta)\dot{y} + \delta^2 y = H$$
$$\times\{C_{L0}q/2 + [A_1(2\pi St\dot{y}) - A_2(2\pi St\dot{y})^3$$

$$+A_3(2\pi St\dot{y})^5 - A_4(2\pi St\dot{y})^7]\}, \quad (6)$$
$$\ddot{q} + \varepsilon\left(q^2 - 1\right)\dot{q} + q = f(y), \quad (7)$$

where H is a mass coefficient defined as $H = 1/(8\pi^2 St^2\mu)$, and () now stands for the derivative with respect to the dimensionless time t. Here, ε is a parameter that is related to the growth in time of the wake oscillation, starting from rest. This corresponds to twice the growth rate of the unstable wake mode, see [31]. The parameter should be set as $0 < \varepsilon < 1$ to make sure it can model a self-sustained stable quasi-harmonic oscillation of finite amplitude [30]. We use here a value of $\varepsilon = 0.3$. This is identical to the value used for circular cylinders in [10] and is consistent with the growth rate of the wake mode behind a square cylinder computed by [32], using the DNS and a linear stability analysis.

3 Forced vibrations

Let us consider a forced oscillation of a square cylinder, $y = y_0\cos(\omega t)$, where y_0 is the dimensionless amplitude and ω represents the angular frequency scaled by the vortex shedding frequency, ω_f. We look for a first harmonic approximation for the function of q, which can be expressed as $q = q_0\cos(\omega t + \theta)$, where θ denotes the phase angle between q and the motion.

3.1 Acceleration coupled model

The only undefined term left in present model is $f(y)$ which may depend on the displacement, the velocity or the acceleration of the structural motion. The acceleration coupling model has been shown to better predict the VIV of a circular cylinder than displacement or velocity; see Facchinetti et al. [10]. For this reason, we first try

$$\ddot{q} + \varepsilon\left(q^2 - 1\right)\dot{q} + q = B_1\ddot{y}. \quad (8)$$

The coupling parameter B_1 scales the effect of the motion of the body on the wake variable, which is the vortex-induced lift. The value of B_1 can be estimated from data of forced vibration experiments as was done in [10] for the circular cylinder case. This is based on the results of some experiments, that the vortex-induced lift is magnified by an imposed structure motion, particularly at resonance [33]. Now, substituting the two

terms $y = y_0\cos(\omega t)$ and $q = q_0\cos(\omega t + \theta)$ into Eq. (8), and considering only the main harmonic contribution of the nonlinearities, we have

$$q_0^6 - 8q_0^4 + 16\left[1 + \left(\frac{\omega^2 - 1}{\varepsilon\omega}\right)^2\right]q_0^2 = 16\left(\frac{B_1 y_0\omega}{\varepsilon}\right)^2, \tag{9}$$

$$\theta = \arctan\frac{\varepsilon\omega}{\omega^2 - 1}(q_0^2/4 - 1). \tag{10}$$

There is unique positive real root in the bi-cubic polynomial of q_0, and it can be obtained numerically. Thus, the instantaneous lift coefficient related vortices can be derived as, $C_L^v = qC_{L0}/2 = q_0 C_{L0}\cos(\omega t + \theta)/2$. To further compare with experiments we now build the whole fluid force applied on the moving square cylinder, combining the wake oscillator terms and the QST terms. In the reduced form of lift coefficient, this reads,

$$C_L^t = C_L^v + C_L^g - C_L^a, \tag{11}$$

where C_L^t is the total lift coefficient and C_L^v is defined above. Here, C_L^a represents the added mass effects that can be expressed here as

$$C_L^a = -\omega^2 C_M 2\pi^3 St^2 y_0\cos(\omega t), \tag{12}$$

where C_M denotes the added mass coefficient, which is mainly related to the cross-section shape and derived from potential flow theory [1]. For a square cylinder, $C_M = 1.51$ (see [1,34]).

The lift coefficient related to galloping, C_L^g, can be computed by substituting $y = y_0\cos(\omega t)$ in Eq. (3),

$$C_L^g = \left[-2\pi St y_0\omega A_1 + (2\pi St y_0\omega)^3\frac{3}{4}A_2\right.$$
$$\left. - (2\pi St y_0\omega)^5\frac{5}{8}A_3 + (2\pi St y_0\omega)^7\frac{35}{64}A_4\right]\sin(\omega t). \tag{13}$$

Then, after elementary algebra, the total lift coefficient can be rewritten as $C_L^t = R\cos(\omega t + \Theta)$, where R and Θ are given by

$$R^2 = (0.5C_{L0}q_0\cos\theta + \omega^2 C_M 2\pi^3 St^2 y_0)^2$$
$$+ \left[-0.5C_{L0}q_0\sin\theta - 2\pi St y_0\omega A_1 + (2\pi St y_0\omega)^3\right.$$
$$\left.\frac{3}{4}A_2 - (2\pi St y_0\omega)^5\frac{5}{8}A_3 + (2\pi St y_0\omega)^7\frac{35}{64}A_4\right]^2,$$

$$\tan\Theta = [-0.5C_{L0}q_0\sin\theta$$
$$-2\pi St y_0\omega A_1 + (2\pi St y_0\omega)^3\cdot$$
$$\frac{3}{4}A_2 - (2\pi St y_0\omega)^5\frac{5}{8}A_3 + (2\pi St y_0\omega)^7\frac{35}{64}A_4\right]$$
$$/(0.5C_{L0}q_0\cos\theta + \omega^2 C_M 2\pi^3 St^2 y_0). \tag{14}$$

Redefining the reduced velocity $U_r = 1/(\omega St)$ for forced vibration, the lift coefficient amplitude, R, and phase angle, Θ, with respect to U_r can be obtained. Figure 2 shows the comparison between the theoretical predictions and experimental data [35] under forced vibration, and the effects of acceleration coupling term B_1 on the unsteady aerodynamic force are also plotted. The coefficients A_i used here are taken from Freda et al. [36] and the $C_{L0} = 1.4$ following the [37], while other parameters are taken from the experimental studies conducted by Carassale et al. [35]. As can be seen from Fig. 2a, a peak value of the amplitude of lift coefficient occurs near $U_r = 1/S_t$, which corresponds to the lock-in region. In addition, increasing B_1 will result in a higher maximum peak of R and a wider range of lock-in region; it therefore means the amplitude R can be probably modelled by this approach. However, in terms of phase angle, the present model is not able to capture enough details in particular at low reduced velocity. The phase angle, Θ, between the cylinder motion and transverse force is quite crucial for predicting VIV and galloping responses, as it determines the energy transfer between structure and fluid. More specifically, it is from flow to cylinder if $0° < \Theta < 180°$, while the energy transfers from cylinder to flow when $-180° < \Theta < 0°$. For this reason, the acceleration coupling term may not be suitable to simulate flow-induced vibrations of a square cylinder because it fails to predict the important characteristics of the phase angle.

3.2 Acceleration and velocity coupled model

An out-of-phase term (velocity coupling term) therefore needs to be taken into account in the form of $f(\dot{y})$ to match the phase angle. A similar method has also been used by several studies [24,26–29]. Then, the Eq. (7) can be rewritten as

$$\ddot{q} + \varepsilon\left(q^2 - 1\right)\dot{q} + q = B_1\ddot{y} + B_2\dot{y}, \tag{15}$$
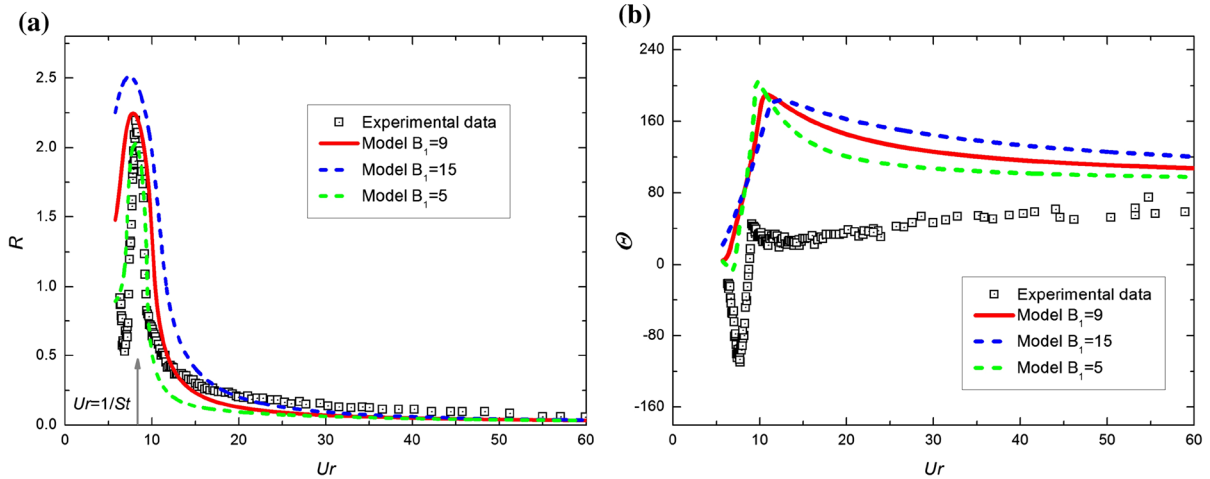
(a)

(b)

Fig. 2 **a** Amplitude of lift coefficient, R, and **b** phase angle, Θ, of a square cylinder under forced vibrations ($y_0 = 0.1$) for several values of the coupling coefficient, B_1. Experimental data are taken from Carassale et al. [35]. Coefficients: $A_1 = 3.01$, $A_2 = 110$, $A_3 = 3037$ and $A_4 = 26, 215$ [36]

where B_1, B_2 are the multiplying factors for acceleration coupling ($B_1\ddot{y}$) and velocity coupling ($B_2\dot{y}$), respectively. Their values can be determined through experiments of forced vibrations as in Sect. 3.1. According to the new term in Eq. (15), the polynomial of q_0 and its phase angle, θ, now read

$$q_0^6 - 8q_0^4 + 16\left[1 + \left(\frac{\omega^2 - 1}{\varepsilon\omega}\right)^2\right]q_0^2$$

$$= 16\left(\frac{B_1 y_0 \omega}{\varepsilon}\right)^2 + 16\left(\frac{B_2 y_0}{\varepsilon}\right)^2, \qquad (16)$$

$$\theta = \arctan\frac{\varepsilon\omega}{\omega^2 - 1}(q_0^2/4 - 1) + \arctan\frac{B_2\omega}{-B_1\omega^2}. \qquad (17)$$

Figure 3 shows the theoretical amplitude of lift coefficient, R, and the phase angle, Θ, by solving Eqs. (16), (17) and (14). The experimental data taken from different forced vibration conditions are also plotted in figures for comparisons [35]. The parameter B_1 affects the variation of the lift coefficient in both maximum peak amplitude and the range of resonance region, while the value of velocity coupling term B_2 does not affect the lift coefficient amplitude. As expected, adding the outphase term in Eq. (15) gives a better predictions for the phase angle than the single accreditation coupling model. Overall, $B_1 = 10$ and $B_2 = 0.1$ are reasonable values for Eq. (15), which can basically match the maximum lift coefficient around the resonance region and accurately capture the variation of both amplitude and

phase angle. Thus, the acceleration and velocity coupled model with these parameters is now used, and they will be applied to the subsequent cases where the square cylinder is set to freely move, without any tuning. In addition, note that our model allows to have, as in the experiments, the value of the critical reduced velocity for zero phase lag that increases with the amplitude y_0 ($U_r^c = 10; 11.2; 12.2, y_0 = 0.1; 0.2; 0.3$). This important point will be discussed later.

4 Free vibrations

We now apply the present model, with the coefficients obtained above from forced vibration experiments, to other experiments where the square cylinder is left free to vibrate. The two Eqs. (6) and (15) are now solved simultaneously with a second order accuracy, with one initial condition on y. Only the limit cycle oscillation is analyzed in terms of magnitude defined by, $\bar{y} = \sqrt{2}y_{rms}$.

An elastically supported square cylinder under flow may vibrate in different ways according to the relationship between the critical reduced velocity for VIV (U_v) and for galloping (U_g). The velocity U_v is associated with the Strouhal number defined as, $U_v = 1/S_t$, while U_g can be obtained by the quasi-steady theory, defined as, $U_g = 8\pi m^* \zeta / A_1$ [19]. The ratio of the two critical velocities reads simply
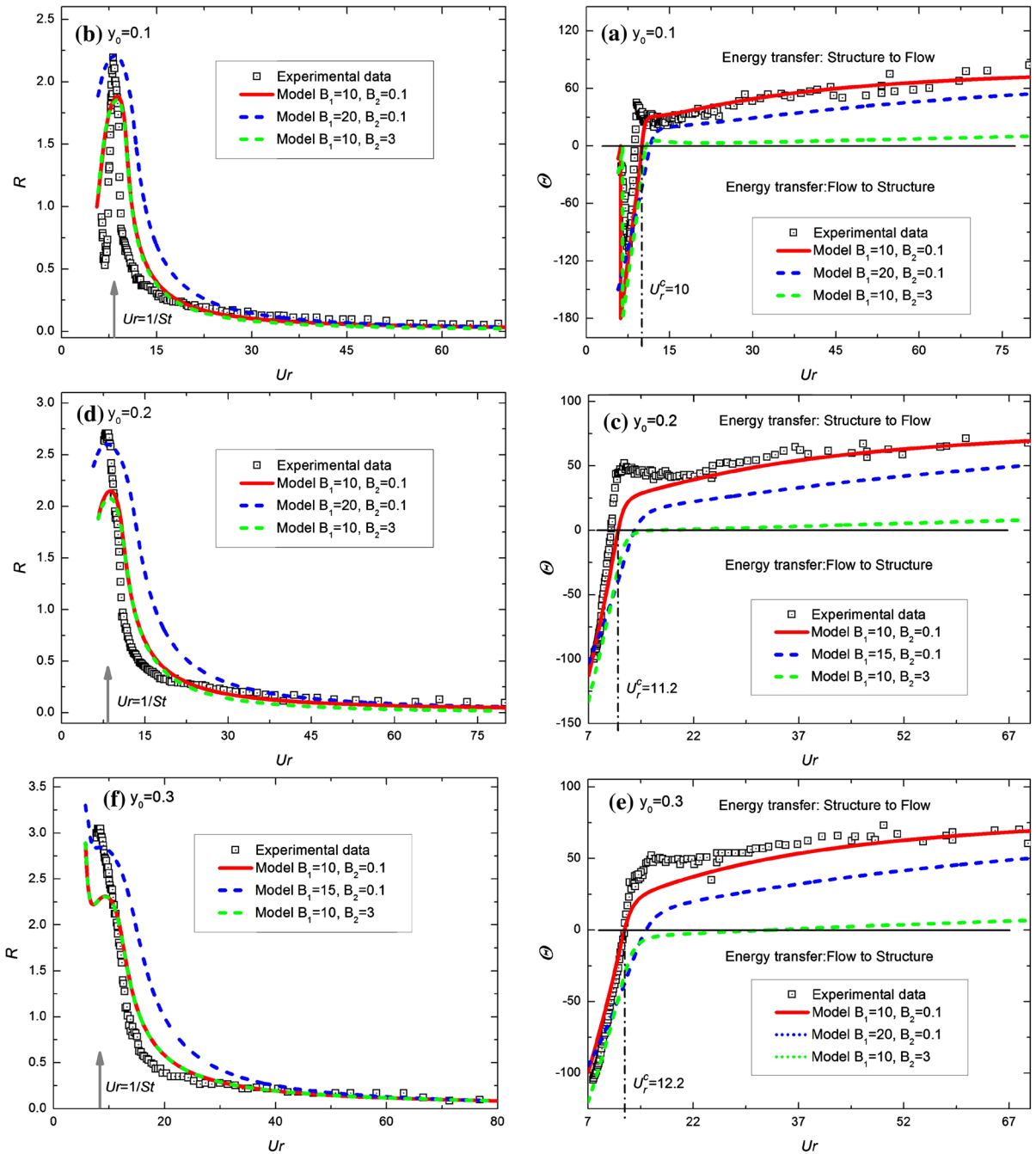
Fig. 3 **b**, **d** and **f** Amplitude of lift coefficient, R, and **a**, **c** and **e** phase angle, Θ, of a square cylinder under different forced vibrations ($y_0 = 0.1$, 0.2 and 0.3). Experimental data are taken from Carassale et al. [35]. The black solid lines in right three figures represent $\Theta = 0$. Coefficients: $A_1 = 3.01$, $A_2 = 110$, $A_3 = 3037$ and $A_4 = 26$, 215 [36]

$$U_g/U_v = 8\pi S_t m^* \zeta / A_1 = 2 S_t S_c / A_1, \tag{18}$$

where A_1 is the first coefficient of the polynomial, Eq. (3), measured by the slope at zero incidence of the

approximated lift coefficient curve. It is a function of both shape and Reynolds number. For a given flow condition on a square cylinder, both A_1 and S_t are fixed,

so that the ratio U_g/U_v only depends on the Scruton number.

4.1 High Scruton number cases

The model is first employed to predict VIV and galloping of a square cylinder at high Scruton numbers. If S_c is high enough, we have $U_g/U_v \gg 1$, and the square cylinder is expected vibrate in "pure VIV" and "pure galloping" at low and high reduced velocity, respectively. Parkinson and Smith have conducted experiments on galloping of a square cylinder [19]. In their work, the mass ratio μ is 1162.8 with different damping ratios ζ varying from 0.00107 to 0.00372. So we can calculate S_c between 15.64 and 54.36, and the ratio U_g/U_v from 1.56 to 5.46. Figure 4 shows the numerical results and the experimental data for comparison. All parameters used for the model are taken from the experiments. The X-axis in Fig. 4 is shown as U_r/U_g, so that the galloping instability should start near $X = 1$. The experimental points plotted in the figure consist of data tested with three different Scruton numbers, and they strongly overlap. Similarly, the predictions by the model give almost identical results for the three Sc conditions, and we only show the curve for the highest value of Sc for clarity. Quite accurate quantitative agreement between numerical data and experiments can be found. In addition, by changing the initial ampli-
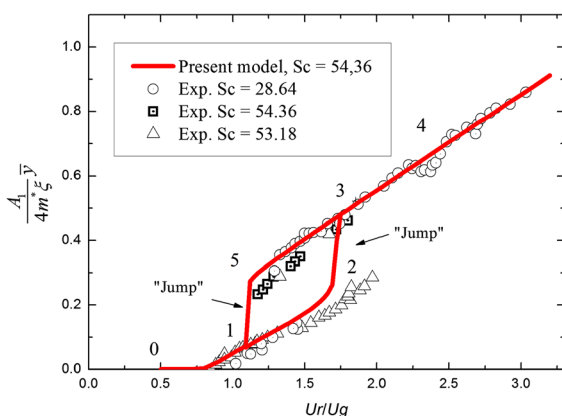

Fig. 4 Pure galloping: Comparison of amplitude responses between experimental and numerical results obtained by present model for S_c=54.36. Experimental data are taken from Parkinson and Smith [19]. Coefficients: $A_1 = 2.69$, $A_2 = 168$, $A_3 = 6270$ and $A_4 = 59,900$ [19]
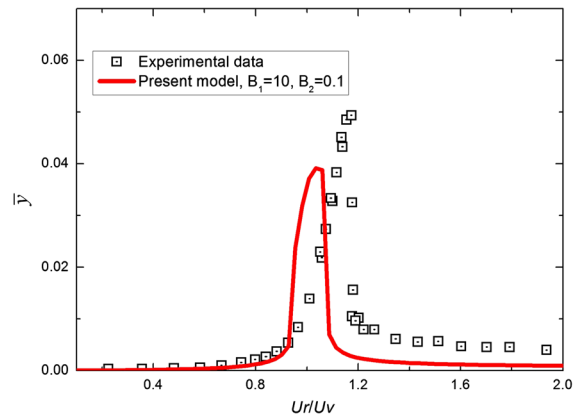

Fig. 5 Pure VIV of a 3:2 rectangular cylinder: Comparison of amplitude responses between experimental and numerical results obtained by present model for S_c=87.7. Experimental data are taken from Mannini et al. [28]. Coefficients: $A_1 = 4.88$, $A_2 = 290.09$, $A_3 = 30140$, $A_4 = 1.1173 \times 10^6$, $A_5 = 1.773 \times 10^7$ and $A_6 = 8.749 \times 10^7$ [28]

tude, we can clearly capture the two "jumps" from point 2 to point 3 and from point 5 to point 1, respectively.

A square cylinder under flow with high S_c is expected to undergo "pure VIV" at low reduced velocity. Very few experiments exist on VIV of square sections at high Scruton numbers. Cheng et al. [39] as well as Amandolèse and Hémon [40] carried out experimental studies on the VIV of a square cylinder, but the S_c in their works are 15.7 and 9.41, respectively, which are not high enough to rule away the influence from galloping. Mannini et al. [28] experimentally and numerically investigated the vibrations of a rectangular cylinder under flow. They tested very high S_c cases (87.7) in wind tunnel and compared the data with results obtained by Corless and Parkinson's model [26] as well as Tamura and Shimada's model [27]. The rectangular cylinder also has leading-edge corners, as the square shape, and there are no significant differences in terms of fluid dynamics between the two geometries. Therefore, it is reasonable to test the present model for "pure VIV" by comparing with experiments of VIV of a rectangular cylinder. The numerical results are plotted in Fig. 5. Note that, the quasi-steady polynomial used here is 11th-order instead of seventh-order following [28]. The S_t, m^*, ξ, C_{L0} and polynomial coefficients A_i can be found in Mannini et al.'s work [28]. As can be seen from Fig. 5, the amplitude predictions agree with the wind-tunnel data, though there are some differences in maximum peak value and the lock-in range. These

differences may caused by the coupling parameters B_1 and B_2 which were determined under forced vibrations of a square cylinder instead of a 3:2 rectangular one. Also, these differences may be caused by the values of S_t and C_{L0} which are not measured at the Reynolds number of lock-in range (see [28]). In conclusion, the model proposed in this paper can reasonably predict the "pure VIV" and "pure galloping" dynamics of a square cylinder under flow.

4.2 Low Scruton number cases

Vortex-induced vibration and galloping can not be totally separated unless the Scruton number is high enough ($U_g/U_v \gg 1$). In most of engineering applications in particular in the cases of hydroelastic oscillations, U_g/U_v is never much greater than 1 because of the fluid density.

Here, the present model is employed to simulate the combined VIV-galloping motions. The numerical predictions are compared with experimental data from Bearman et al. [38] and Wawzonek [22] in Fig. 6a and b. Note that, the values of S_c are 11.76 ($U_g/U_v = 0.63$) and 31.98 ($U_g/U_v = 1.92$), respectively. For the lower one, U_g is less than U_v, so that VIV and galloping are strongly coupled. Parameters used for this case can be found in [26]. As shown in Fig. 6a, the present numerical results are close to the experiments.

However, there are two branches with different limit cycle oscillations in the amplitude curve, which are not observed in the experiments. This is probably because the experiments are conducted with a cylinder starting from rest only. For the case of Fig. 6b, U_g/U_v is larger than 1 but not much. Although Fig. 6b apparently shows a VIV motion and a galloping motion (separate VIV-galloping), the two phenomena are actually weakly coupled. The model parameters for this case are the same as the experiments cited in Fig. 6b, aside from the $C_{L0} = 0.6$ which is not mentioned in their work. Figure 6a and b shows that when the interactions between VIV and galloping cannot be ignored, the critical velocity for galloping instability (compared with U_g derived from quasi-steady theory) is reduced. The phenomenon is important for engineering applications because it may cause unexpected vibrations for structures if only considering U_g in the design. This indicates that the quasi-steady theory is not suitable to simulate galloping (particularly its critical value) in low S_c number cases. Finally, the critical reduced velocity of instability as well as the interactions between VIV and galloping, including combined and separate VIV-galloping motions, are successfully captured by the present model. Overall, the model predict well the vibrations of a square cylinder, though the amplitudes in VIV part are slightly overestimated.
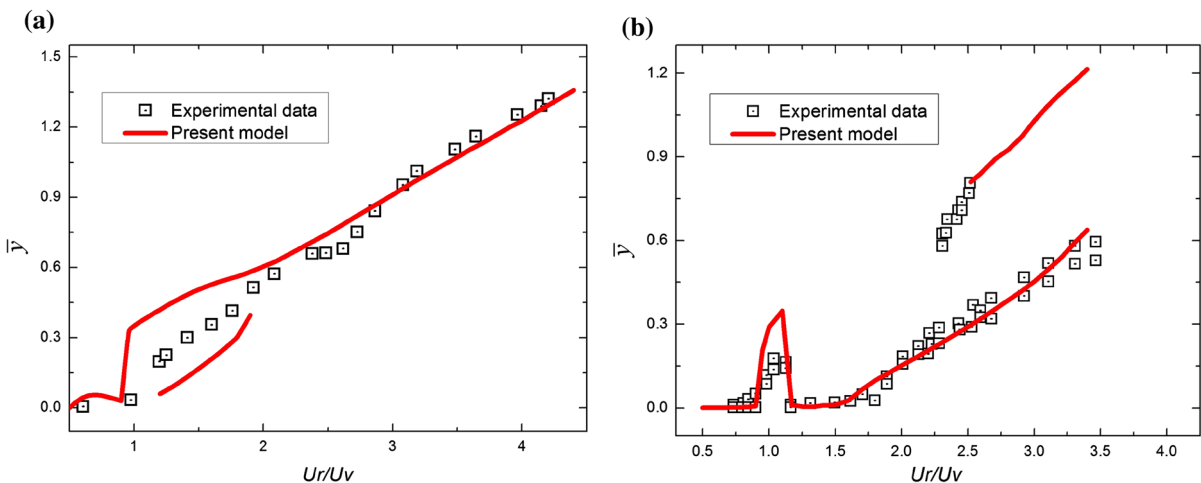

Fig. 6 Comparison between experimental results and numerical predictions obtained by the present model for (**a**) $S_c = 11.76$ (strongly coupled VIV-galloping) and (**b**) $S_c = 31.98$ (weakly coupled VIV-galloping). Experimental data in (a) and (b) are taken from Bearman et al. [38] and Wawzonek [22], respectively. Coefficients (**a**): $A_1 = 4.87$, $A_2 = 421$, $A_3 = 17,000$ and $A_4 = 194,000$ [26]. Coefficients (**b**): $A_1 = 4$, $A_2 = 260$, $A_3 = 10,000$ and $A_4 = 100,000$ [22]

5 Discussion

Before the present model, two models were mostly used to predict transverse oscillation of a square cylinder, of which one is Corless and Parkinson's model [26] and the other is Tamura and Shimada's model [27]. In fact, the form of the present model is similar to those two models, for instance, all the three models use the acceleration & velocity coupling terms. However, the present model still differs from others in some aspects. First, the added mass effects are considered in the present model. Second, the flow variable q satisfies a standard van der Pol equation, while it is Rayleigh equation for Corless and Parkinson's model and the parameters in their model lack physical meaning. Third, the ability to simulate phase angle of a square cylinder under flow are obviously different for the three models. A comparison between theoretical results with experimental data for the phase angle is plotted in Fig. 7. Note that, the experimental data we used for this comparison is different from that in Fig. 3. The flow parameters, i.e., C_{L0}, A_i, and S_t, used for the three compared models are same, and they are taken from the existing literature [19,41]. It can be found that the present model matches the experiments more accurately than the other two models. Moreover, as mentioned in Sect. 3.2, the present model clearly captures the change in sign of the phase. As reported by Liu et al. [29], this is not properly captured by existing
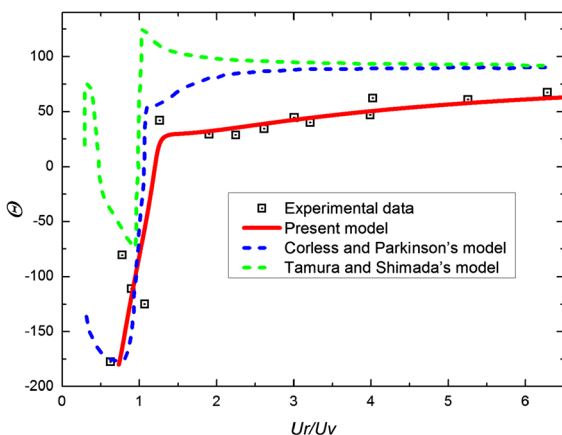

Fig. 8 Pure VIV case: comparison between experimental and numerical results obtained with different models for S_c=87.7. Red solid line: Present model with quasi-steady coefficients A_i that taken from [28]. ⊙: Present model with quasi-steady coefficients, A_i (except A_1) set to zero. Experimental data are taken from Mannini et al. [28]

models. It is nevertheless an important feature for the oscillation of a square cylinder, because it can affect the amplitude of VIV by limiting the excitation; see [3]. Finally, because the differences among the three models occur in the force term related to VIV, we plot the predictions with different models for "pure VIV" of a 3:2 rectangular in Fig. 8 for comparison. All the coupling parameters or the model parameters used here are from a square cylinder, which means ε, B_1 and B_2 are same as the previous cases and the parameters used for Corless and Parkinson's model and Tamura and Shimada's model are directly taken from their work without any tuning [26,27]. Other parameters applied for the three compared models, i.e., the mass ratio μ and the damping ratio ξ for the structure; C_{L0}, A_i and S_t for the flow, are exactly the same, and they are all taken from the experiments [28]. The results show that the present model provides more reasonable predictions on both the maximum amplitude and the lock-in range. In addition, for Tamura and Shimada's model, though the empirical model parameters are given physical meanings, it is more difficult to extend to other cases because extra experiments may be needed to estimate the parameters' values, see [27]. The above evidences indicate that the present model may be easier to applied in other cases.

Amandolèse and Hémon experimentally investigated VIV of a square cylinder at Re = 2000–8000 [40]. The present model does not predict such vibration as

Fig. 7 Comparison of the phase angle between lift and motion predicted by different models with experiments. Experimental data are taken from Nakamura and Mizota, $y_0 = 0.1$ [41]. Coefficients: $A_1 = 2.69$, $A_2 = 168$, $A_3 = 6270$ and $A_4 = 59,900$ [19]
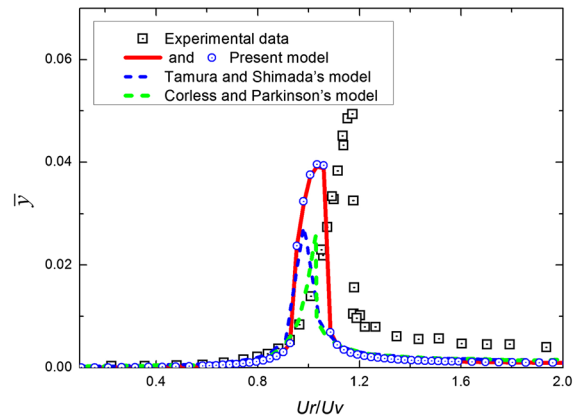
successfully as expected, though we have all the parameters in the VIV part. This is because although the cylinder in their work seems vibrating in separated VIV-galloping motion, in fact, the S_c is 9.41 which is low. Therefore, interactions between VIV and galloping potentially affect the vibration responses. However, we lack data on the coefficients A_i for the quasi-steady polynomial in that low Re range. For this case, changing the A_i will not only change the galloping responses, but also significantly alter the maximum amplitude and lock-in range among resonance region. This proves VIV of a square cylinder with low S_c can not be simulated by single wake oscillator model that only considers vortex force. Conversely, in the high S_c cases, as shown in Fig. 8, the amplitude responses are almost unchanged if all the coefficients A_i (expect A_1) are set to zero. The above evidences indicate that the present model can be used to compute a critical value for S_c (or U_g/U_v), which determines whether the interactions between VIV and galloping are negligible. Over the critical S_c, VIV and galloping of a square cylinder can be predicted separately; otherwise, the two force terms related to vortices and the flow need to be coupled.

There are some guidelines or steps for applying the present model to other free vibration cases. First, the parameters C_{L0}, S_t and A_i, related respectively to oscillating lift, vortex-shedding frequency and lift on a fixed cylinder need to be determined by experiments or simulations. (i) The parameters C_{L0} and S_t are obtained from the case of the incidence angle equals to zero; (ii) a polynomial approximation of the effect of the incidence angle α on the lift gives the coefficients A_i. The free oscillation responses for given structural parameters (i.e., the mass ratio μ and damping ratio ξ) can then be obtained by solving Eqs. (6) and (15).

The present model may have some limitations in its use, for instance, (i) in terms of damping of the structural mode, the case of zero damping is particular: The quasi-steady model would predict a galloping instability that starts at zero flow velocity, which is not physically appropriate. (ii) in terms of Reynolds number, the model incorporates the Reynolds number effect in the coefficients. Still, when the mechanism represented by the elements of the model do not follow the simple rules of Eqs. (6) and (15), the model is not adequate. For instance, at very low Reynolds number in the absence of vortex shedding, Eq. (15) is pointless and the parameter C_{L0} should be put to zero. (iii) if the incoming flow velocity is relatively small and the galloping instability

occurs, i.e. the motion for the square cylinder is not "slow" when compared with the incoming flow, the quasi-steady theory approximation is less valid. Thus, the present coupled model that combines wake oscillator and QST becomes less accurate. This is for instance probably the cause of the overestimate of the amplitude of motion in Fig. 6a.

6 Conclusions

To conclude, a new approach for the transverse oscillation of a square cylinder under flow has been proposed. The unsteady lift forces were determined by combining: (i) the incidence angle effects using the quasi-steady theory, (ii) the vortex force described by a nonlinear wake oscillator, as well as (iii) the added mass effects. The wake oscillator model and the QST model use coefficients (B_1, B_2, C_{L0}, S_t) and (A_i) that are to be determined from specific test (or computation) conditions. Coefficients B_1 and B_2 are obtained from the fluid loading under forced oscillation. Coefficients C_{L0}, S_t and A_i are determined by lift measurement on fixed bodies under varying angles of attack, of which C_{L0} and S_t are obtained by a particular case with incidence angle equals to zero. The above coefficients are then used to try and reproduce the behavior of a square free to move.

Examining the model by comparison with experiments shows that it can effectively predict both vibration and forces characteristics, including: (a) lift coefficient and phase angle variations under forced vibration; (free vibrations) high S_c cases including (b) "pure galloping" and (c) "pure VIV"; (d) interactions between VIV and galloping, including combined and separate VIV-galloping vibrations. The present model is simple to use and may easily be extended to other flow conditions, shapes, and flexible cylinders. In addition, this model is helpful to understand the underlying mechanics between VIV and galloping, and it can identify the critical Scruton number for the VIV-galloping interactions.

References

1. Blevins, R.D.: Flow-Induced Vibration. Krieger Publishing Company, Florida (1977)
2. Parkinson, G.V.: Phenomena and modelling of flow-induced vibrations of bluff bodies. Prog. Aerosp. Sci. **26**(2), 169–224 (1989)
3. Bearman, P.W.: Vortex shedding from oscillating bluff bodies. Ann. Rev. Fluid Mech. **16**(1), 195–222 (1984)
4. Williamson, C.H.K., Govardhan, R.: Vortex-induced vibrations. Ann. Rev. Fluid Mech. **36**(1), 413–455 (2004)
5. Sarpkaya, T.: A critical review of the intrinsic nature of vortex-induced vibrations. J. Fluids Struct. **19**(4), 389–447 (2004)
6. Lucor, D., Foo, J., Karniadakis, G.E.: Vortex mode selection of a rigid cylinder subject to VIV at low mass-damping. J. Fluids Struct. **20**(4), 483–503 (2005)
7. Hartlen, R.T., Currie, I.G.: Lift-oscillator model of vortex-induced vibration. J. Eng. Mech. Div. **EM5**, 577–591 (1970)
8. Skop, R.A., Balasubramanian, S.: A new twist on an old model for vortex-excited vibrations. J. Fluids Struct. **11**(4), 395–412 (1997)
9. Abdelkefi, A., Hajj, M.R., Nayfeh, A.H.: Phenomena and modeling of piezoelectric energy harvesting from freely oscillating cylinders. Nonlinear Dyn. **70**(2), 1377–1388 (2012)
10. Facchinetti, M.L., de Langre, E., Biolley, F.: Coupling of structure and wake oscillators in vortex-induced vibrations. J. Fluids Struct. **19**(2), 123–140 (2004)
11. Facchinetti, M.L., de Langre, E., Biolley, F.: Vortex-induced travelling waves along a cable. Eur. J. Mech. B/Fluids **23**(1), 199–208 (2004)
12. Violette, R., de Langre, E., Szydlowski, J.: Computation of vortex-induced vibrations of long structures using a wake oscillator model: comparison with dns and experiments. Comput. Struct. **85**(11–14), 1134–1141 (2007)
13. Grouthier, C., Michelin, S., Bourguet, R., Modarres-Sadeghi, Y., de Langre, E.: On the efficiency of energy harvesting using vortex-induced vibrations of cables. J. Fluids Struct. **49**, 427–440 (2014)
14. Zanganeh, H., Srinil, N.: Three-dimensional VIV prediction model for a long flexible cylinder with axial dynamics and mean drag magnifications. J. Fluids Struct. **66**, 127–146 (2016)
15. Gabbai, R.D., Benaroya, H.: An overview of modeling and experiments of vortex-induced vibration of circular cylinders. J. Sound Vib. **282**(3–5), 575–616 (2005)
16. Tamura, Y., Matsui, G.: Wake-oscillator model of vortex-induced oscillation of circular cylinder. In: Proceedings of the 5th international conference on wind engineering, pp. 1085–1094, Bowness-on-Windermere, (1980)
17. Benaroya, H., Gabbai, R.D.: Modelling vortex-induced fluid-structure interaction. Philos. Trans. A Math. Phys. Eng. Sci. **366**(1868), 1231–74 (2008)
18. Meliga, P., Chomaz, J.-M.: An asymptotic expansion for the vortex-induced vibrations of a circular cylinder. J. Fluid Mech. **671**, 137–167 (2011)
19. Parkinson, G.V., Smith, J.D.: The square prism as an aeroelastic non-linear oscillator. Q. J. Mech. Appl. Math. **17**(2), 225–239 (1964)
20. Joly, A., Etienne, S., Pelletier, D.: Galloping of square cylinders in cross-flow at low reynolds numbers. J. Fluids Struct. **28**, 232–243 (2012)
21. Norberg, C.: Flow around rectangular cylinders: pressure forces and wake frequencies. J. Wind Eng. Ind. Aerodyn. **49**(1), 187–196 (1993)
22. Wawzonek, M. A.: Aeroelastic behavior of square section prisms in uniform flow. PhD thesis, University of British Columbia (1979)
23. Abdelkefi, A., Hajj, M.R., Nayfeh, A.H.: Power harvesting from transverse galloping of square cylinder. Nonlinear Dyn. **70**(2), 1355–1363 (2012)
24. Andrianne, T., Aryoputro, R.P., Laurent, P., Colson, G., Amandolèse, X., Hémon, P.: Energy harvesting from different aeroelastic instabilities of a square cylinder. J. Wind Eng. Ind. Aerodyn. **172**, 164–169 (2018)
25. Bouclin, D. N.: Hydroelastic oscillations of square cylinders. PhD thesis, University of British Columbia (1979)
26. Corless, R.M., Parkinson, G.V.: A model of the combined effects of vortex-induced oscillation and galloping. J. Fluids Struct. **2**(3), 203–220 (1988)
27. Tamura, Y., Shimada, K.: A mathematical model for the transverse oscillations of square cylinders. In: Proceedings of the 1st international conference on flow induced vibrations, pp. 267–276, Bowness-on-Windermere (1987)
28. Mannini, C., Massai, T., Marra, A.M., Bartoli, G.: Modelling the interaction of VIV and galloping for rectangular cylinders. In: The 14th international conference on wind engineering, pp. 1–20, Porto Alegre (2015)
29. Liu, Y.Z., Ma, C.M., Li, Q.S., Yan, B.W., Liao, H.L.: A new modeling approach for transversely oscillating square-section cylinders. J. Fluids Struct. **81**, 492–513 (2018)
30. Nayfeh, A.H.: Introduction to Perturbation Techniques. John Wiley & Sons, New Jersey (2011)
31. de Langre, E.: Frequency lock-in is caused by coupled-mode flutter. J. Fluids Struct. **22**(6–7), 783–791 (2006)
32. Li, X., Lyu, Z., Kou, J., Zhang, W.: Mode competition in galloping of a square cylinder at low reynolds number. J. Fluid Mech. **867**, 516–555 (2019)
33. Bishop, R.E.D., Hassan, A.Y.: The lift and drag forces on a circular cylinder in a flowing fluid. Proc. R. Soc. Lond. Ser. A Math. Phys. Sci. **277**(1368), 32–50 (1964)
34. Luo, S.C., Bearman, P.W.: Predictions of fluctuating lift on a transversely oscillating square-section cylinder. J. Fluids Struct. **4**(2), 219–228 (1990)
35. Carassale, A., Freda, L., Banfi, L.: Motion excited forces acting on a square prism: a qualitative analysis. In: The 14th international conference on wind engineering, Porto Alegre (2015)
36. Freda, A., Carassale, L., Piccardo, G.: Aeroelastic cross-wind response of sharp-edge square sections: experiments versus theory. In: The 14th international conference on wind engineering, 01 (2015)
37. Carassale, L., Freda, A., Marrè-Brunenghi, M.: Experimental investigation on the aerodynamic behavior of square cylinders with rounded corners. J. Fluids Struct. **44**, 195–204 (2014)
38. Bearman, P.W., Gartshore, I.S., Maull, D.J., Parkinson, G.V.: Experiments on flow-induced vibration of a square-section cylinder. J. Fluids Struct. **1**(1), 19–34 (1987)

39. Cheng, L., Zhou, Y., Zhang, M.M.: Perturbed interaction between vortex shedding and induced vibration. J. Fluids Struct. **17**(7), 887–901 (2003)
40. Amandolèse, X., Hémon, P.: Vortex-induced vibration of a square cylinder in wind tunnel. Comptes Rendus Méc. **338**(1), 12–17 (2010)
41. Nakamura, Y., Mizota, T.: Unsteady lifts and wakes of oscillating rectangular prisms. J. Eng. Mech. Div. **101**, 855–871 (1975)